ACS OMEGA

http://pubs.acs.org/journal/acsodf
Article

Dielectric Barrier Discharge Plasma Processing and Sr-Doped ZnO/CNT Photocatalyst Decoration of Cotton Fabrics for Self-Cleaning Application

Mabkhoot Alsaiari, Saba Afzal, Ameer Sultan, Shazia Shukrullah,* Muhammad Saleem, Muhammad Yasin Naz,* Moustafa A. Rizk, and Muhammad Irfan

Cite This: *ACS Omega* 2024, 9, 1977−1989

ABSTRACT: Nonthermal plasma processing is a chemical-free and environmentally friendly technique to enhance the self-cleaning activity of nanoparticle-coated cotton fabrics. In this research, Sr-doped ZnO/carbon nanotube (CNT) photocatalysts, namely, $S_{10}ZC_2$, $S_{15}ZC_2$, and $S_{20}ZC_2$ with different Sr doping concentrations, were synthesized using the sol−gel method and coated on plasma-functionalized fabric to perform the self-cleaning tests. The fabrics were treated with dielectric barrier discharge plasma in an open environment for 3 min to achieve a stable coating of nanoparticles. The energy band gap of the photocatalyst decreased with an increase in the level of Sr doping. The band gap of $S_{10}ZC_2$, $S_{15}ZC_2$, and $S_{20}ZC_2$ photocatalysts was estimated to be 2.85, 2.78, and 2.5 eV, respectively. The hexagonal wurtzite structure of ZnO was observed on the fabric surface composited with CNTs and Sr. The $S_{20}ZC_2$ photocatalyst showed better homogeneity and photocatalytic response on the fabric when compared with $S_{10}ZC_2$- and $S_{15}ZC_2$-coated fabrics. The $S_{20}ZC_2$ photocatalyst showed 89% dye degradation efficiency after 4 h of light exposure in methylene blue solution, followed by $S_{15}ZC_2$ (84%) and $S_{10}ZC_2$ (80%) photocatalysts.

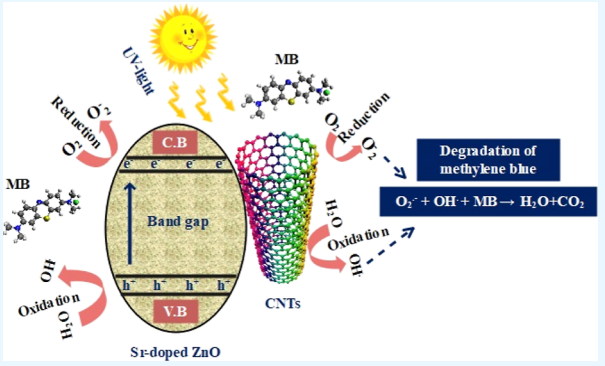

1. INTRODUCTION

Nanotechnology is swiftly attracting global attention because it is widely perceived as offering huge potential in cutting-edge technologies.[1] Nanotechnology and nanoparticles provide numerous benefits in the textile sector, transforming the qualities and capabilities of textiles. Incorporating nanotechnology in textiles is a developing topic with continuing research and development, presenting promise for continued textile industry innovation. Incorporating nanoparticles or nanofibers into textile materials significantly improve their traits like durability, strength, water and stain resistance, UV protection, antibacterial and antimicrobial properties, thermal regulation, smart textiles, color enhancement, self-cleaning fabrics, improved insulation, flexible electronics, etc.[1−3] Conventional nanocoating methods do not produce long-lasting results due to the surface energy difference and lack of adherence between fabric and coated products.[2] A significant aspect of our consumer culture is textiles. Clothing, towels, furniture, carpeting, car interiors, etc. are all made of textiles.[3] Although both synthetic and natural fibers are used in textiles, the chemical processing of the fibers has more adverse health effects than that of the cloth itself. The other chemical treatments and fabric dyeing are the major reasons for health implications and allergic reactions. A new category of self-cleaning fabrics with superhydrophobic qualities is under development.[4] By coating fabrics with pure and mixed metal oxides, self-cleaning textiles can be developed and used with positive effects on human health and the environment.[5] Self-cleaning materials are well known for their high repellency against both oil and water, which easily rip off their surfaces. Due to their great degree of repellency, these materials can come into contact practically with any liquid.[6] Different methods have been used to produce self-cleaning fabrics, including dip-coating, spray coating, spin coating, electro-spraying, electro-spinning, hydrothermal treatment, chemical etching, and vapor deposition.[7] The coating is the chemical application to the fabric's surface, giving it functional and decorative properties.[8] Nearly, all textile products used in hotels and medical facilities cause cross-contamination or the spread of diseases brought on by microorganisms. A common

Received: November 18, 2023
Revised: December 2, 2023
Accepted: December 8, 2023
Published: December 21, 2023

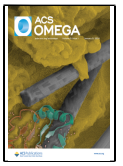

https://doi.org/10.1021/acsomega.3c09207
ACS Omega 2024, 9, 1977−1989

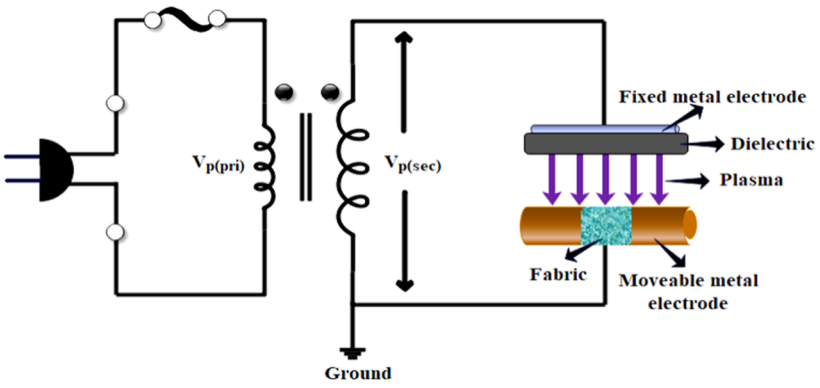

Figure 1. Schematic of the DBD system for processing of fabric.

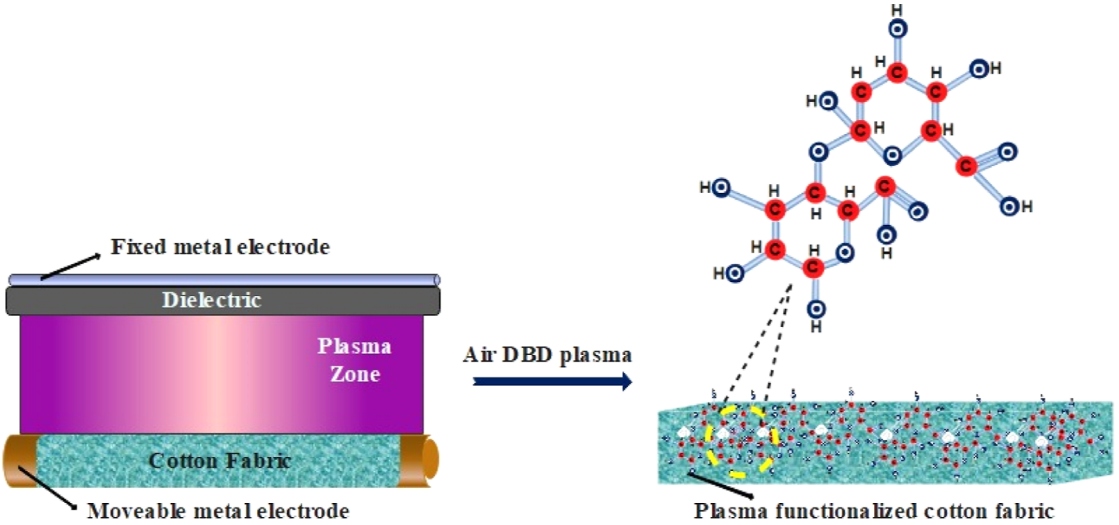

Figure 2. Illustration of the plasma functionalization process of fabrics.

method of coating the fabrics is spraying, washing, transfer printing, rising, and padding. The coating of nanoparticles on fabrics can be performed by a padder adjusting to suitable speed and pressure, followed by curing and drying.[9]

Photocatalysis is a novel technique for eliminating both inorganic and organic pollutants from the atmosphere and water bodies.[10] ZnO is an n-type semiconductor with a 3.37 eV band gap energy, which is a very reliable photocatalyst due to its effectiveness in degrading organic dyes.[11] At the nanoscale, ZnO is an effective and appealing ingredient for sunscreen and cosmetics due to its high UV resistance.[12] Since the band gap of ZnO falls in the UV region of the light spectrum, its effectiveness as a photocatalyst depends on factors such as particle size, active surface area, and crystalline structure. Efforts are being made to address challenges such as recombining electron−hole pairs, which can limit the overall efficiency of photocatalytic processes involving ZnO. The large surface area, excellent stability, low mass density, and low electrical resistance of carbon nanotubes (CNTs) make them good electrically conductive materials. Substrate materials become conductive after CNTs are coated on the textile.[13,14] The addition of Sr to the photocatalyst can further enhance the ionic properties of the photocatalyst during a photocatalytic process.[15] Saleem et al.[16] revealed that the ultrasonic biosynthesis of TiO_2 nanoparticles for decorating the plasma pretreated cotton fabric improves wettability and self-cleaning efficiency. The plasma treatment on the cotton fabric was performed by dielectric barrier discharge (DBD) plasma to enhance self-cleaning activity. The color pixel difference was used to check the degradation of 0.05% MB dye solution after 15 h of reaction time under sunlight. Irfan et al.[17] worked on ultrasonically ZnO loading of plasma-citric acid-modified cotton fabric for self-cleaning, antibacterial, and UV protection activities. They achieved a methylene blue dye degradation efficiency of 77% using ZnO-loaded fabric. In another study, Saleem et al.[18] enhanced the photocatalytic efficiency of TiO_2 on fabrics by compositing it with Cu_2O. They plasma functionalized the fabrics and coated them with Cu_2O/TiO_2 composites. The plasma processing and Cu_2O/TiO_2 coating resulted in 94% photocatalytic efficiency of the processed fabrics. Plasma treatment also contributes to the stability and photocatalytic effectiveness of a catalyst on the fabric surface.[19]

The plasma exposure of textiles improves the surface roughness and induction rate of functional groups, which are key drivers in nano finishing and photocatalytic applications of textiles. Çakır et al.[20] plasma processed the fabrics to produce ZnO-coated textiles. They revealed that plasma-processed textiles showed good wettability, adhesion, and durability for coating applications. Through ionization and dissociation processes, plasma produces reactive species on cotton fabric. These species not only play a role in the bonding of nanoparticles with the fabric surface but also contribute to the self-cleaning and antibacterial traits of the fabrics. This study aimed at plasma processing of cotton fabrics for the

https://doi.org/10.1021/acsomega.3c09207
ACS Omega 2024, 9, 1977−1989

Figure 3. Illustration of procedures involved in the production of Sr-doped ZnO/CNTs.

production of efficient Sr/ZnO/CNTs composite-coated textiles for self-cleaning application. The Sr-doped ZnO/CNTs with different doping concentrations of Sr were prepared through the sol−gel route and coated onto plasma-processed fabrics using the pad-dry method.[21] The self-cleaning tests with the nanocoated fabrics were performed in a methylene blue solution under sunlight.

2. MATERIALS AND METHODS

2.1. Chemicals. Zinc nitrate ($Zn(NO_3)_2$), strontium nitrate ($Sr(NO_3)_2$), citric acid ($C_6H_8O_7$), sodium hydroxide (NaOH), carbon nanotubes (CNTs), distilled water, acetone (C_3H_6O), and methylene blue (MB) were used in completing this research work.

2.2. DBD Plasma System. A self-sustained DBD plasma discharge was produced under atmospheric pressure conditions, as illustrated in Figure 1. The air in the surroundings was considered a working gas for plasma microdischarge. DBD system consisted of a pair of metal electrodes: one was fixed, while the other cylindrical electrode was rotatable. The fixed electrode was covered with a dielectric tube, while the rotatable electrode was covered with a fabric sample.[22] A 30 kV alternating current supply with a variac and 60 Hz cycle provided the current in mA for plasma generation.[23] The plasma operating conditions include a 40 mA discharge current at 20 kV discharge voltage, an interelectrode gap of 3 mm, and a plasma activation time of 5 min. The source gas was air since DBD was sustained in an open atmosphere. Before the plasma processing, fabric samples were washed with acetone to remove the seizing particles and dried at 90 °C in an oven for 120 min. The fabric was pasted on the motor-driven movable cylindrical electrode for the plasma treatment, as illustrated in Figure 2.

The DBD discharge was produced with the above-mentioned fixed process conditions with air as the working gas for plasma production. Plasma was used to activate the fabric surface for an exposure time of 5 min. The reactive species generated in the plasma-induced reactions on the fabric surface as illustrated in Figure 2. For instance, they broke the existing chemical bonds and formed new bonds, introducing new functional groups. Oxygen and nitrogen-containing groups, such as hydroxyl, carbonyl, carboxyl, and amino groups, can be introduced onto the surface, enhancing its reactivity. The process of most common radicals formed during plasma processing is defined in eq 1.

$$5H_2O \rightarrow 2OH + e^- + H + H_2O_2 + H_3O + H_2 \quad (1)$$

A few highly energetic electrons collide with oxygen (O_2) molecules in the air. Due to their tendency to react, the O_2 molecules transform into atomic oxygen (O) and produce ozone and reactive hydroxyl (OH) radicals, as explained in eqs 2 and 3.

$$O_2 + O \rightarrow O_3 \quad (2)$$

$$O_2 \rightarrow 2O \rightarrow 2OH \quad (3)$$

2.3. Preparation of Photocatalyst-Coated Fabrics. Sr-doped ZnO/CNTs photocatalysts were produced using a facile sol−gel method and coated over plasma-functionalized fabrics to observe the self-cleaning activity, as illustrated in Figure 3. The nanoparticles of ZnO were prepared by adding 4.17 g of zinc nitrate and 10 g of citric acid in 100 mL of distilled water under mild stirring and heating for 45 min. The resulting solution was collected in a crucible and dried in an oven at 120 °C for 24 h, followed by calcination in the furnace. The white solid powder was cooled to room temperature and ground into a fine ZnO powder. The formation of Sr-doped ZnO/CNTs photocatalyst was performed with the same method as ZnO by adding 0.82 g or 10 wt % of strontium nitrate to the solution. Then, the solution was introduced with 2 wt % of CNTs and labeled as solution-A. The base solution-B was prepared by adding NaOH to deionized water. Solution B was added dropwise to solution A to maintain pH at 9 and get solution C. The gel formed on stirring the solution-C for 3 h was collected in a crucible and dried at 120 °C before calcinating for 24 h at 400 °C. The final product was crushed into fine powder to get $S_{10}ZC$ photocatalyst. Two more photocatalyst samples, namely, $S_{15}ZC_2$ and $S_{20}ZC_2$, were prepared using 1.09 and 1.35 g of strontium nitrate, respectively. A description of the prepared samples is provided in Table 1.

To establish a self-cleaning feature in the fabric, the prepared $S_{10}ZC_2$, $S_{15}ZC_2$, and $S_{20}ZC_2$ photocatalysts were coated on plasma-activated fabric samples. The fabric samples of 6 × 6 cm^2 size were dipped in a 15 mL solution of binder and the photocatalyst. The coated samples were passed through the pad dry machine for the homogeneous and stabilized coating. Then, the coated fabrics were gently washed to remove the extra particles that could not make solid contact with the

https://doi.org/10.1021/acsomega.3c09207
ACS Omega 2024, 9, 1977−1989

Table 1. Description of Photocatalysts with the Sr Doping Percentage

sample	Sr content (wt %)	CNT content (wt %)
$S_{10}ZC_2$	10	2
$S_{15}ZC_2$	15	2
$S_{20}ZC_2$	20	2

sample. The samples were dried for 1 h at 70 °C. Figure 4 explains the procedure of the pad dry coating process used in this work.[24,25]

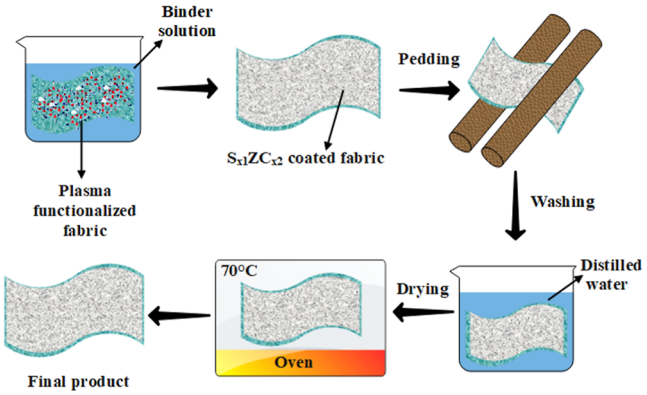

Figure 4. Explanation of the pad-dry process for producing nanocoated fabrics.

2.4. Self-Cleaning Activity. The self-cleaning performance of the prepared fabric samples was checked by decolorizing the MB dye solution under solar irradiation, as illustrated in Figure 5. The $S_{10}ZC_2$-, $S_{15}ZC_2$-, and $S_{20}ZC_2$-coated fabrics were immersed in a 0.05% solution of MB dye and placed under sunlight for 4 h.[5,26] Thereafter, the photocatalyst-decorated fabric samples were removed from the dye solution, washed with deionized water, and dried in an oven for 1 h at 70 °C. The dye degradation efficiency of the nanocoated fabrics was calculated using the following eq 4

$$\text{degradation efficiency } (\%) = \left[1 - \frac{C}{C_0}\right] \times 100 \quad (4)$$

where C and C_0 are the concentrations of dye after and before irradiation.

3. RESULTS AND DISCUSSION

3.1. Analysis of Functional Groups. The functional groups and chemical bonds of dye and photocatalysts on the fabric surface were checked from FTIR spectra. The peak at 1632 cm^{-1} represents C═N central ring stretching and the peak at 3300 cm^{-1} represents NH/−OH overlapped stretching vibration in the structure of MB dye, as reported in Figure 6a. Figure 6b depicts FTIR spectra of the photocatalyst-decorated fabrics in the range of 500−4000 cm^{-1}, which represent the presence of metals and CNTs in the composite photocatalyst.[27] Four prominent peaks were observed in the FTIR spectra at 697, 1158, 2953, and 1434 cm^{-1}. The peaks at 697, 1158, and 2953 cm^{-1} were observed at the same wavenumber for $S_{15}ZC_2$ and $S_{20}ZC_2$ composite-coated samples in the group frequency region (GFR) and fingerprint region (FPR). The peak at 697 cm^{-1} confirmed the presence of halo compounds, such as the C−X bond where "X" is known as halogen (X = Br, Cl, F, and I) within the range of 850−550 cm^{-1}. In this FPR, the peak at 697 cm^{-1} demonstrated the C−Cl vibration frequency with a strong peak appearance.[28] A tertiary alcohol group is shown with a peak at 1158 cm^{-1}, which also has a significant appearance in the FPR. At this peak, the C−O stretching vibration of alcohol shows the presence of one or more carbon atoms and is known as symmetric and asymmetric C−C−O stretching.[29]

The peak at 2953 cm^{-1} was observed in the GFR with three different compound classes, carboxylic acid, alcohol, amine salt, and alkane. These compounds showed strong broad, weak broad, and medium appearances with O−H stretching, N−H stretching, and C−H stretching vibrations, respectively.[30] The peak at 1434 cm^{-1} was noted only for $S_{10}ZC_2$ composite with a medium appearance due to O−H bending of the carboxylic acid class in FPR, as mentioned in Table 2. Similarly, there are two further peaks at 1632 and 3300 cm^{-1} for MB that also appeared in FPR and GPR, respectively. When compared with 1632 cm^{-1}, the peak at 3300 cm^{-1} exhibits a strong appearance, indicating that there is a large amount of energy absorbed at this frequency.

3.2. Structural Analysis. XRD spectra of $S_{10}ZC_2$-, $S_{15}ZC_2$-, and $S_{20}ZC_2$-decorated fabrics are reported in Figure 7. XRD peaks at 2θ of 7, 32.5, 34.7, 40.3, and 44.6° correspond to (002), (100), (002), (100), and (101) diffraction planes. The characteristic peaks at 7, 40.3, and 44.6° showed the presence of CNTs in the photocatalysts.[31] These peaks correspond to Miller indices of (002), (100), and (101) in

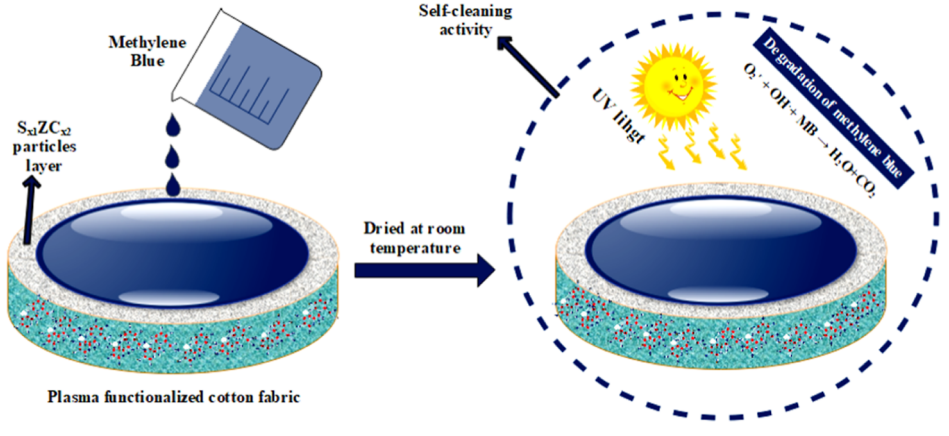

Figure 5. Dye degradation mechanism of nanocoated fabrics under sunlight.

https://doi.org/10.1021/acsomega.3c09207
ACS Omega 2024, 9, 1977−1989

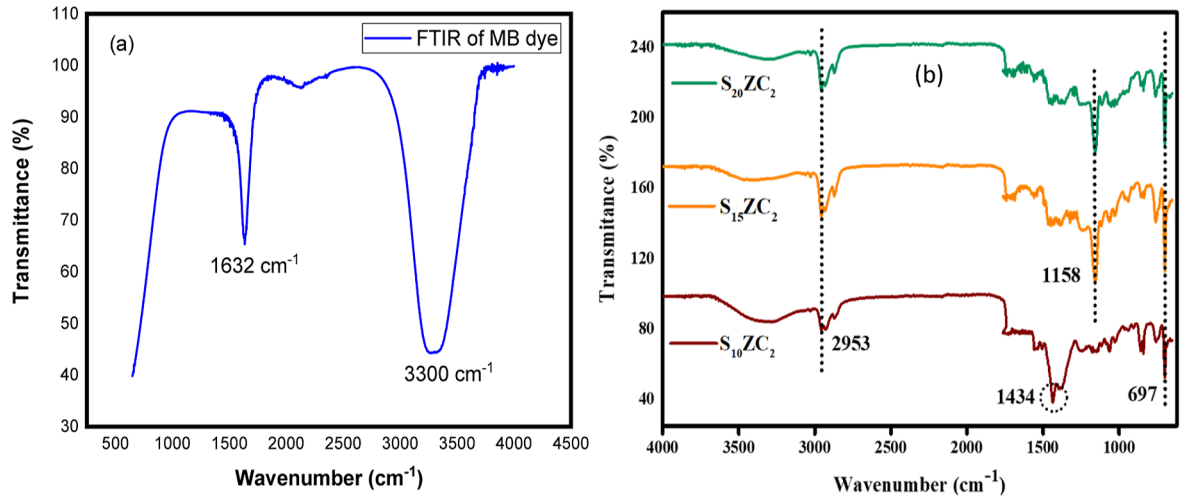

Figure 6. (a) FTIR pattern of MB dye and (b) FTIR spectra of $S_{10}ZC_2$-, $S_{15}ZC_2$-, and $S_{20}ZC_2$-decorated fabrics.

Table 2. FTIR Peaks with Corresponding Functional Groups and Compounds of Photocatalysts

wavenumber (cm^{-1})	groups	compounds class	peaks appearance	group region
697	C−Cl stretching	halo compound	strong	FPR
1632	C═C stretching	alkene	medium	GFR
3300	O−H stretching	alcohol	strong	GFR
1434	O−H bending	carboxylic acid	medium	FPR
2953	O−H stretching, C −H stretching, N −H stretching	carboxylic acid, alkane alcohol, amine salt	strong broad medium weak broad	GFR
1158	C−O stretching	tertiary alcohol	strong	FPR

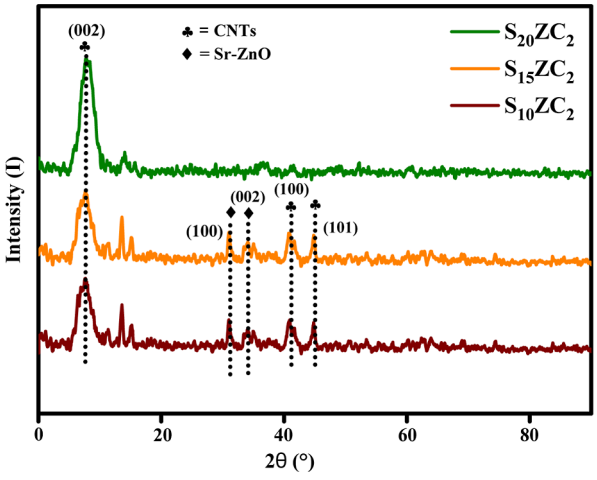

Figure 7. XRD spectra of $S_{10}ZC_2$-, $S_{15}ZC_2$-, and $S_{20}ZC_2$-decorated fabrics.

the $S_{10}ZC_2$ and $S_{15}ZC_2$ photocatalysts. The JCPDS no. 26-1076 also confirms the peaks of CNTs. The structural analysis agreed with the findings of Geetha et al.[32] The $S_{10}ZC_2$ and $S_{15}ZC_2$-decorated fabrics also revealed two peaks at 31.9 and 34.7°, which were perceived as the (100) and (002) planes, respectively, according to JCPDS no. 36-1451.[33] The ionic radius of Zn^{2+} (0.074 nm) is less than that of Sr^{2+} (0.118 nm). When Sr is doped into the ZnO structure, Sr^{2+} ions distort the host lattice of zinc (Zn^{2+}) and cause the peaks to shift. However, in this case, the diffraction peaks were hardly shifted toward higher 2θ values. The distortion was limited to a small region, causing no shift in XRD peaks. This analysis also showed the hexagonal wurtzite crystal structure of ZnO (JCPDS no. 36-1451).[34] The Scherrer formula was used to determine the grain size of the $S_{10}ZC_2$, $S_{15}ZC_2$, and $S_{20}ZC_2$ photocatalysts. The grain size, *d*-spacing values, and Miller indices of all three photocatalysts are given in Table 3.

Table 3. Structure Parameters Were Determined through XRD Analysis of the Photocatalyst-Decorated Fabrics

photocatalyst	2θ°	indices (*hkl*)	grain size (nm)	*d*-spacing (Å)
		For Characteristic Peaks		
$S_{10}ZC_2$	7	(002)	12.05	0.69
$S_{15}ZC_2$	7	(002)	12.05	0.60
$S_{20}ZC_2$	7	(002)	12.05	0.69
		For Other Peaks		
$S_{10}ZC_2$	32.5	(100)	7.7	2.7
	34.7	(002)	8.96	2.62
	40.3	(100)	12.2	2.23
	44.6	(101)	8.98	2.02
$S_{15}ZC_2$	32.5	(100)	7.7	2.7
	34.7	(002)	8.96	2.62
	40.3	(100)	12.2	2.23
	44.6	(101)	8.98	2.02

3.3. UV−Visible Spectroscopy Analysis. The UV−visible spectra of the $S_{10}ZC_2$, $S_{15}ZC_2$, and $S_{20}ZC_2$ photocatalysts are presented in Figure 8a. The photoabsorption peaks of these photocatalysts underwent a redshift at wavelengths of 366, 367, and 396 nm, respectively. The combined impact of Sr^{2+} and CNTs changed the local structure of ZnO, which increased the flow of electric charge carriers to the composite surface.[35] The absorbance intensity and the corresponding band gap energy of the prepared photocatalysts are given in Table 4. The optical band gap of photocatalysts reduced with an increase in Sr doping concentration, indicating a synergic effect of Sr-doped ZnO and CNTs. Figure 8b−d provides a relation of Kubelka−Munk $[\alpha h\nu = A\cdot(h\nu - E_g)^{n/2}]$ used for the estimation of the optical band gap energy of the photocatalysts. The $S_{10}ZC_2$, $S_{15}ZC_2$, and $S_{20}ZC_2$ photocatalysts showed a band gap energy of 2.85, 2.78, and 2.5 eV, respectively.[36]

https://doi.org/10.1021/acsomega.3c09207
ACS Omega 2024, 9, 1977−1989

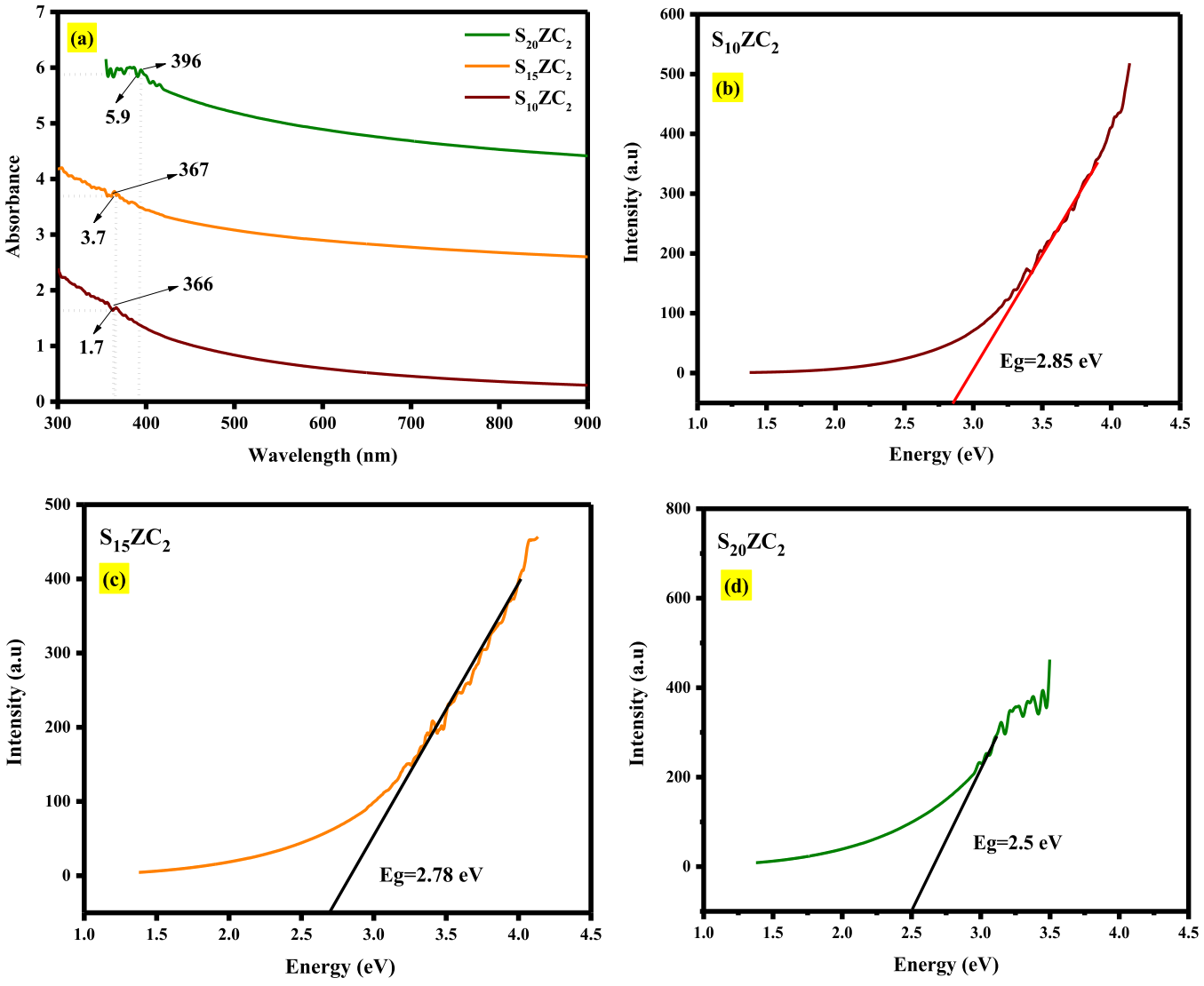

Figure 8. (a) UV−visible absorbance spectra of $S_{10}ZC_2$, $S_{15}ZC_2$, and $S_{20}ZC_2$, and band gap energy of (b) $S_{10}ZC_2$, (c) $S_{15}ZC_2$, and (d) $S_{20}ZC_2$ photocatalysts.

Table 4. Light Absorbance and Band Gap Energy Values of the Photocatalysts

photocatalyst	wavelength (nm)	absorbance	band energy (eV)
$S_{10}ZC_2$	366	1.7	2.85
$S_{15}ZC_2$	367	3.7	2.78
$S_{20}ZC_2$	396	5.9	2.5

3.4. Surface Morphology of Photocatalyst Finished Fabrics. Figure 9 depicts the surface morphologies of $S_{10}ZC_2$, $S_{15}ZC_2$, and $S_{20}ZC_2$ photocatalysts. Figure 9a shows the hard-rock-like structure of ZnO nanoparticles with undefined boundaries. Measuring the particle size or shape from this clustered growth of the nanostructures is difficult. This morphology turned into a spongy matric with the addition of Sr at different concentrations, as shown in Figure 9b. Some needle-like structures were also observed in Sr-doped ZnO. These Sr needles make the structure spongy and increase the reactive surface area of the catalyst. The photocatalyst was then mixed with CNTs as a charge sink and catalyst support. Figure 9c shows the size distribution of CNTs used as a catalyst support. The average diameter of CNTs remained around 57 nm. CNTs were fully covered with photocatalyst particles. The vertically aligned CNTs in Figure 9d ensure better charge transport properties than those having mixed orientations.[37−39] The composite photocatalysts were decorated over plasma process fabrics through the pad dry method.

Figure 10a,b shows SEM images of photocatalyst-decorated fabric without a CNTs support. The fibers were uniformly covered with photocatalyst powder. The reactive surface of this sample was much smaller than those having CNTs in the catalyst composition. Figure 10c,d shows fibers covered with a Sr-doped ZnO/CNT photocatalyst. The magnified image in Figure 10d shows the forest-like growth of the catalyst on the fiber surface. The photocatalyst-decorated CNTs grow from the fiber surface and provide a large contact area for photocatalytic activity. When Sr-doped ZnO and CNTs are mixed, they may display synergistic effects, in which the qualities of the separate components are increased. Compared to the individual components, this synergy can improve overall catalytic performance. CNTs are well known for their high electrical conductivity. Incorporating CNTs into Sr-doped ZnO catalysts can improve the catalyst's electron transport characteristics. This is critical for catalytic reactions that

https://doi.org/10.1021/acsomega.3c09207
ACS Omega 2024, 9, 1977−1989

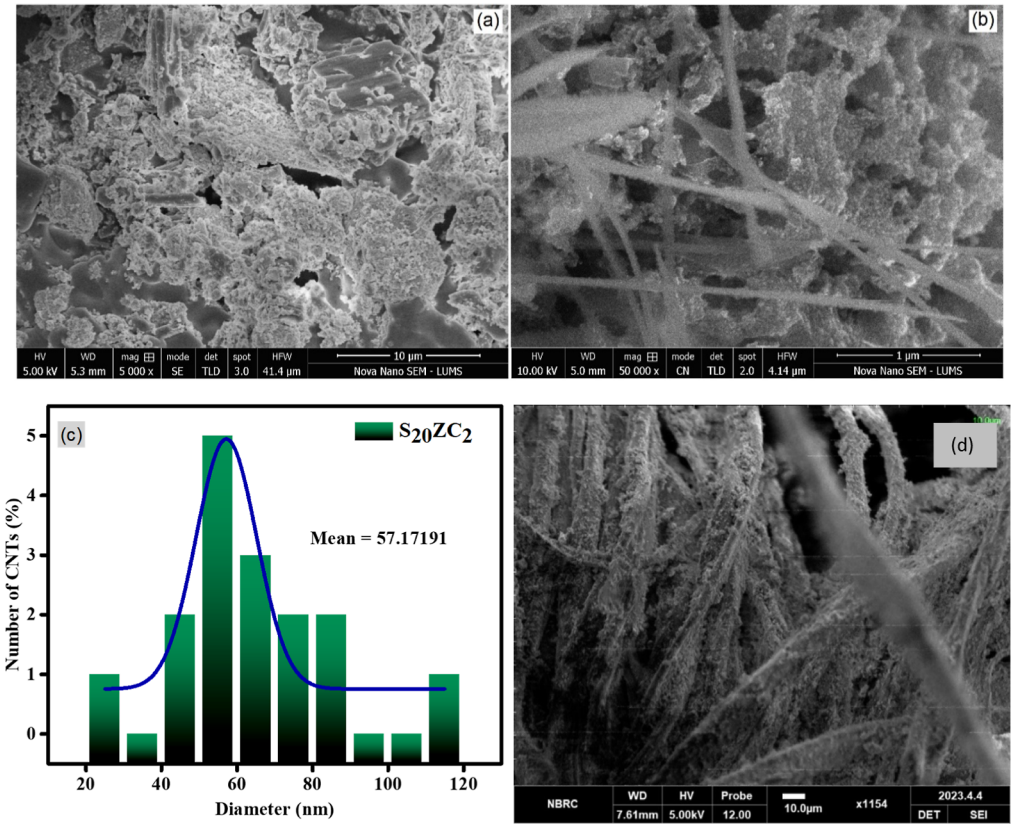

Figure 9. (a) SEM image of ZnO, (b) SEM of Sr-doped ZnO, (c) diameter distribution of CNTs, and (d) SEM image of Sr-doped ZnO/CNT photocatalyst.

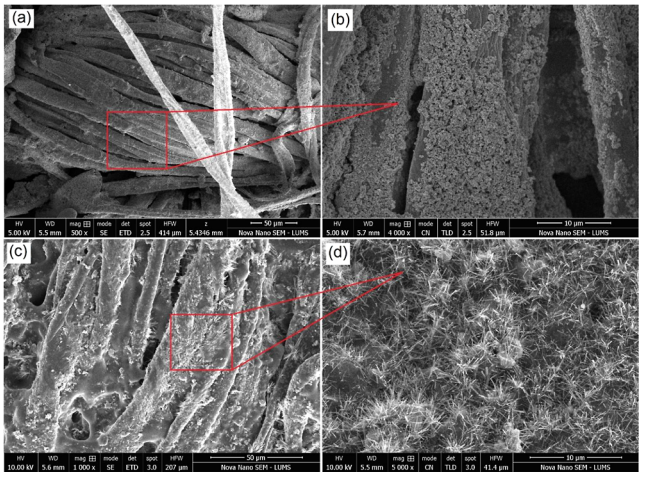

Figure 10. (a,b) SEM images of Sr-doped ZnO-decorated fabric and (c,d) SEM images of Sr-doped ZnO/CNT-decorated fabric.

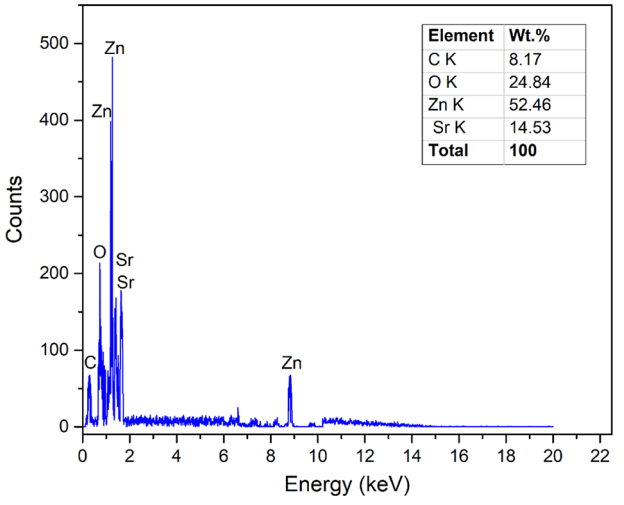

Figure 11. Typical EDX spectrum of the Sr-doped ZnO/CNT photocatalyst.

involve electron transfer steps because it promotes efficient charge transfer and decreases electron−hole recombination. Because of their typical structure, CNTs have a large surface area. This increased surface area may result in more active sites for catalytic reactions, leading to greater catalytic activity.

EDX analysis of the composite photocatalyst was performed to confirm its elemental composition. A typical EDX spectrum in Figure 11 confirmed the presence of C, O, Zn, and Sr elements in the composite photocatalyst. These elements were found in 8.17, 24.84, 52.46, and 14.53 wt % in the photocatalyst, respectively. The presence and distribution of these elements can provide insights into the composition and structure of the material. The elemental composition of Sr-doped ZnO/CNT composite depends on the specific synthesis conditions and the intended doping levels. The synergistic action of Sr-doped ZnO and CNTs can result in a catalyst with improved reactant accessibility to active sites. CNTs can be used to assist the dispersion of Sr-doped ZnO nanoparticles. This can avoid nanoparticle aggregation and guarantee a uniform distribution of active sites on the catalyst surface. Better dispersion can result in improved catalytic efficiency and selectivity. The plasma-induced cracks and pits due to the

https://doi.org/10.1021/acsomega.3c09207
ACS Omega 2024, 9, 1977−1989

etching effect also enhance the adsorption and stability of nanoparticles on the fabric.[16] The induction of the functional groups (−COOH and −OH) on the fabric shows a strong electrostatic interaction with the photocatalyst particles.[17−19] The photocatalyst coating was found to be denser and more homogeneous over plasma-processed fabrics than over unprocessed fabrics.

3.5. Self-Cleaning Activity of Finished Fabrics. The photocatalytic activity of the finished fabrics for the self-cleaning application was investigated by exposing the dye solution to light in the presence of a fabric sample. Equation 5 was used to determine the decolorization of dye over time.

$$\left[\ln\frac{C}{C_0}\right] = K_{app}\cdot t \tag{5}$$

where C, K_{app}, and t are the concentration of dye at time t, apparent rate constant, and exposure time, respectively. C_0 is the initial concentration of dye. The graph of dye degradation is plotted between $\left[\ln\frac{C}{C_0}\right]$ and time in Figure 12.[40] The following formula was used to determine the percentage degradation

$$\text{degradation (\%)} = \left(1 - \frac{C}{C_0}\right) \times 100 \tag{6}$$

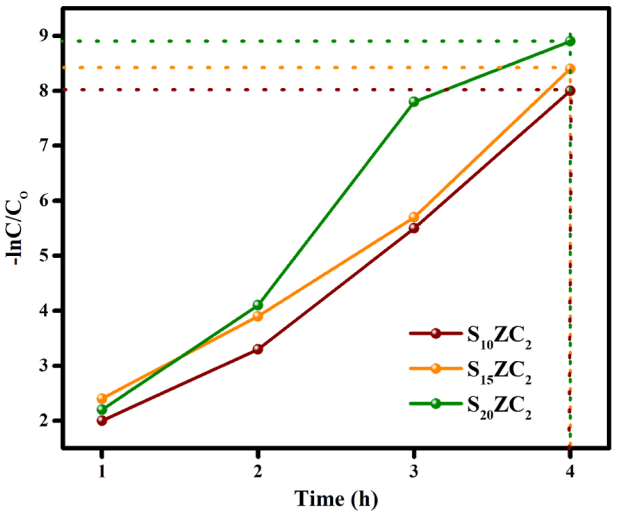

Figure 12. Self-cleaning activity of $S_{10}ZC_2$-, $S_{15}ZC_2$-, and $S_{20}ZC_2$-decorated fabrics in MB dye solution.

In this case, C_0 is the starting concentration of dye and C is the concentration of dye after a specified time. The maximum degradation efficiency of 89% was achieved with $S_{20}ZC_2$-decorated fabric after 4 h of light exposure. The $S_{10}ZC_2$- and $S_{15}ZC_2$-decorated fabrics showed 80 and 84% degradation efficiency, respectively. It shows that degradation efficiency increases with an increase in Sr concentration in the composite photocatalyst.[41]

CNTs in the photocatalyst composition also enhanced the dye degradation rate. Under light irradiation, CNTs inject the electrons into the conduction band of Sr where they form superoxide ($O_2^{\bullet-}$) and hydroxyl radicals ($OH^{\bullet}$). These highly reactive species accelerate redox reactions involved in degrading dye molecules, helping keep fabrics clean.[42] CNTs can operate as electron transport channels, aiding the separation and flow of electrons and holes created during the photocatalytic process. This phenomenon can reduce electron−hole recombination, making the catalyst more efficient at producing reactive oxygen species and, as a result, breaking down the dye molecules. Additionally, the increased surface area of vertically standing CNTs provides extra sites for anchoring the dye molecule. This adsorption can aid in the interaction of dye molecules with photocatalytically active sites on Sr-doped ZnO nanoparticles. Combining adsorption and photocatalysis can result in excellent removal of dye from the catalyst surface.

The other factor affecting the self-cleaning efficiency is the plasma treatment of the fabric.[43] As shown in Figure 13, air was used as a source gas for plasma generation in a DBD arrangement. The charges between the electrodes cannot be transferred from one electrode to another in a single microdischarge due to the dielectric layer between the electrodes. Plasma radicals are generated when a reaction occurs between air molecules and emitted electrons. The mechanism of generating plasma radicals and activating the fabric surface is described by eq 7.[18]

$$5H_2O \xrightarrow{e^-} 2\cdot OH + H_2O_2 + e^- + H_2 + H_3^+O \tag{7}$$

At the same time, the reaction between O_2 and some high-energy electrons takes place in the air. As a result, hydroxyl (OH) radicals are generated due to the dissociation of O_2 into atomic oxygen (O). The UV light is generated by the combination of free radicals and charged species that contribute to the formation of hydroxyl (OH) radicals. These plasma-generated O, O_3, O_2, OH, and H radicals modify cellulose chemistry.[15,19] In cellulose, the dehydrogenation of ribose sugar at the C_6 carbon forms carboxylic acid, which is then oxidized. The hydrophilicity of the fabric increases with the growth of carboxyl groups on cellulose in the form of a molecular chain. The aldehyde groups contribute to the further oxidation of carboxylic acid produced due to the oxidation of primary alcohol during plasma exposure.[19]

3.6. Mechanism of Self-Cleaning Activity. The reaction mechanism of photodegradation of organic dyes on the Sr-doped ZnO/CNT-decorated fabrics is described in Figure 14.[44] The photons with a suitable energy illuminate catalyst nanoparticles. As a result, charge separation and an electron−hole pair are generated. The ZnO nanoparticles in contact with Sr capture the photoinduced e^-_{CB}, as described in eq 8.

$$Sr/ZnO + light \rightarrow Sr(e^-)/ZnO(h^+) \tag{8}$$

At the same time, the holes (h^+) present in ZnO react with the OH^- group and H_2O to produce the hydroxyl radicals ($OH^{\bullet}$).[45] In the same way, the e^- of Sr produces superoxide radicals ($O_2^{\bullet-}$) when it reacts with O_2. The superoxide radicals then degrade dye molecules, as summarized in eqs 9−11.[46,47]

$$ZnO(h^+) + H_2O(H^+ + OH^-) \rightarrow ZnO + H^+ + OH^{\bullet} \tag{9}$$

$$ZnO(h^+) + OH^- \rightarrow ZnO + OH^{\bullet} \tag{10}$$

$$Sr(e^-) + O_2 \rightarrow Sr + O_2^{\bullet-} \tag{11}$$

When electrons from ZnO are transferred to the CNT, they oxidize H_2O_2 into hydroxyl radicals. The reaction mechanism of oxidation of dye starts when light falls on the excited state of the dye, which then injects an electron into the conduction

https://doi.org/10.1021/acsomega.3c09207
ACS Omega 2024, 9, 1977−1989

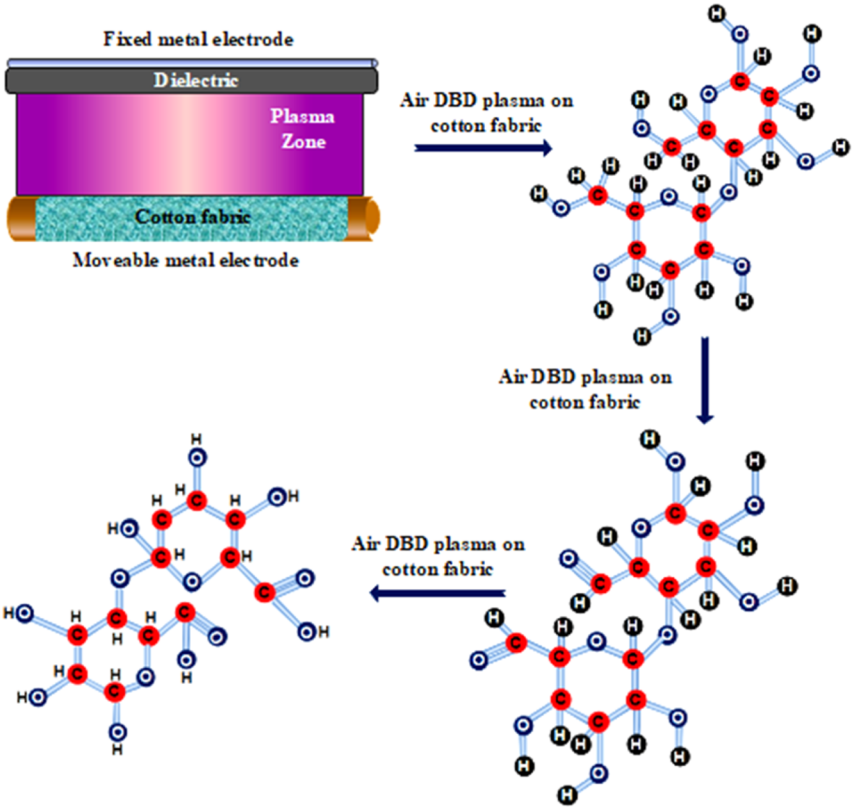

Figure 13. Illustration of the mechanism of plasma processing of the fabric surface.

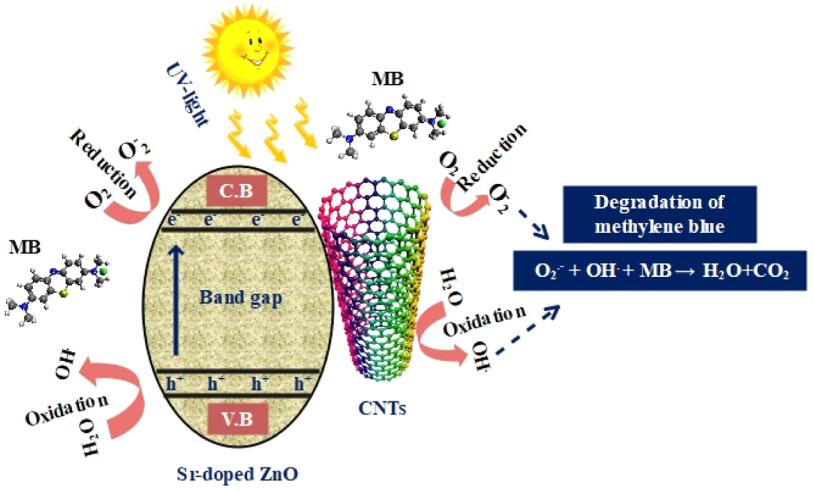

Figure 14. Mechanism of self-cleaning activity of the Sr-doped ZnO/CNT-decorated fabric.

band of Sr. After this excitation, MB dye changes to $MB^{\bullet+}$ known as the catatonic dye radical ion, which takes part in further reactions. As hydroxyl radicals are highly reactive, they generate maximum electrons and holes and are used as a reactant for dye oxidation into environmentally friendly compounds (CO_2 and H_2O), as described by eqs 12−14.[48,49]

$$MB + light \rightarrow MB^{*} \quad (12)$$

$$MB^{*} + Sr \rightarrow MB^{\bullet+}e^{-}(Sr) \quad (13)$$

$$MB^{\bullet+} + OH^{\bullet} + O_2^{\bullet-} \rightarrow degradation \quad (14)$$

The oxidized form of MB has a blue color, while the reduced form (leuco MB) is colorless. Auxochrome and chromophoric groups are responsible for the color of MB. The auxochrome group of MB has N-groups and a lone pair of e^{-1} on the ring of benzene, while the chromophore group consists of an N−S conjugated system on the central aromatic heterocycle. The interaction of light with MB is essential to understanding the light adsorption and photodegradation processes, as most observations are derived from ultraviolet and visible parts of the light spectrum. The absorption peak at 664 nm represents the MB monomer in its absorption spectra while the peak at 612 nm corresponds to MB dimer. Absorption peaks at 292 and 245 nm are attributed to substituted benzene rings. The

https://doi.org/10.1021/acsomega.3c09207
ACS Omega 2024, 9, 1977−1989

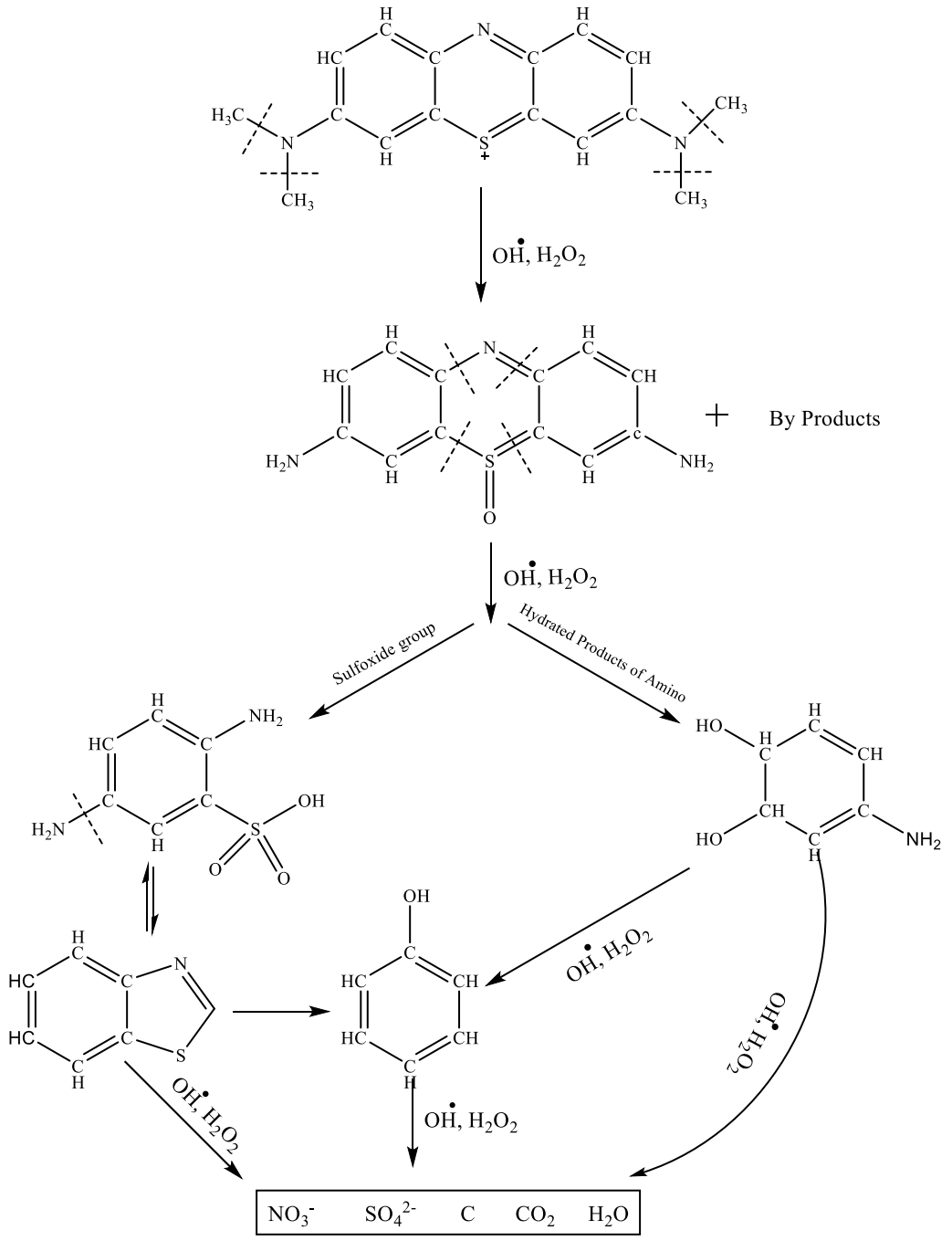

Figure 15. Pathway of degradation of MB dye during the photocatalytic process.

concentration of such peaks decreases as the photodegradation reaction proceeds.

Complete degradation and ring opening of MB take place by $^{\bullet}$OH active species. The functional group "C−S+═C" is attacked by $^{\bullet}$OH to start MB degradation. The transformation from C−S+═C to C−S(═O)−C loses the double bond. The double bond conjugation is conserved by opening the heteroatoms S- and N-containing central aromatic rings. The hole-induced H^+ forms NH and CH bonds. This is the primary cause of the breaking of large molecules into smaller oxidized molecules. FTIR study suggests that $^{\bullet}$OH radicals attack the side chain of MB in the demethylation process. It is also suggested that H_2O_2 and $^{\bullet}$OH are attracted by the heteroaromatic ring and cationic sulfur group of MB that cause the breaking of the cationic sulfur group. In this way, hydroxylated and sulfoxide intermediate products are produced. Such sulfoxide groups oxidize to sulfone and dissociate the other two rings.[49] These aromatic molecules degrade, resulting in the formation of volatile low-molecular-weight chemicals, such as CO_2, H_2O, NH^{4+}, NO_3^-, and SO_4^{2-} ions. The dye degradation mechanism is schematically illustrated in Figure 15.

3.7. Stability and Recyclability Test. The photocatalyst-decorated fabrics are often tested for durability through repeated wash cycles to check their economic value and environmental impact. The number of washes they can withstand without a significant loss of coated material and performance depends on the coating technology and the fabric

https://doi.org/10.1021/acsomega.3c09207
ACS Omega 2024, 9, 1977−1989

itself. For stability testing, the photocatalyst-decorated fabrics were subject to 5 wash cycles in deionized water at room temperature. The coated fabric suffered roughly 11% weight loss due to the removal of nanoparticles from the fabric surface. The weight loss can be higher under real washing conditions, depending on detergent type, temperature, and abrasive washing conditions. The nanocoating showed reasonably high stability in deionized water after multiple cycles. Recyclability is another factor in assessing the economic value of nanofinished fabrics. If a catalyst can be retrieved and reutilized without losing mass or photocatalytic activity, it will add economic value to the process. Therefore, five self-cleaning cycles in the MB solution were performed with the nanocoated fabric. After each cycle, the coated fabric sample was washed in deionized water and dried in an oven for 60 min at 90 °C. The self-cleaning efficiency after the first cycle was recorded as 89%, which reduced to 77% after five cycles. The nanofinished fabrics still showed reasonably good self-cleaning activity after multiple photocatalytic cycles.

4. CONCLUSIONS

The Sr-doped ZnO/CNTs with different doping concentrations of Sr were prepared through the sol−gel route and coated onto plasma-processed fabrics using the pad-dry method.[21] The self-cleaning tests with the nanocoated fabrics were performed in a methylene blue solution under sunlight. A DBD discharge of air was used to activate the fabric surface for an exposure time of 5 min. The plasma-induced cracks and pits enhance the adsorption and stability of nanoparticles on the fabric surface by introducing functional groups (−COOH, −OH) on the fabric. The self-cleaning performance of the prepared fabric samples was checked by decolorizing MB dye solution under solar irradiation for 4 h. The produced catalysts showed an average grain size of less than 12 nm. The band gap of $S_{10}ZC_2$, $S_{15}ZC_2$, and $S_{20}ZC_2$ photocatalysts was estimated to be 2.85, 2.78, and 2.5 eV, respectively. Incorporating CNTs into Sr-doped ZnO catalysts improved the electron transport characteristics of the photocatalyst. The large surface area of CNTs also results in more active sites for catalytic reactions, leading to greater catalytic activity. The $S_{20}ZC_2$ photocatalyst showed 89% dye degradation efficiency after 4 h of light exposure in methylene blue solution, followed by $S_{15}ZC_2$ (84%), and $S_{10}ZC_2$ (80%) photocatalysts. The self-cleaning efficiency underwent a decrease from 89 to 77% after five cycles. The coated fabric showed 11% weight loss after five washing cycles in the deionized water.

■ ASSOCIATED CONTENT

Data Availability Statement

The data that support the findings of this study are available within the article.

■ AUTHOR INFORMATION

Corresponding Authors

Shazia Shukrullah − *Department of Physics, University of Agriculture Faisalabad, Faisalabad 38040, Pakistan*; orcid.org/0000-0002-4474-3768; Email: zshukrullah@gmail.com

Muhammad Yasin Naz − *Department of Physics, University of Agriculture Faisalabad, Faisalabad 38040, Pakistan*; Email: yasin306@uaf.edu.pk

Authors

Mabkhoot Alsaiari − *Empty Quarter Research Unit, Department of Chemistry, Faculty of Science and Arts at Sharurah, Najran University, Sharurah 68342, Saudi Arabia*

Saba Afzal − *Department of Physics, University of Agriculture Faisalabad, Faisalabad 38040, Pakistan*

Ameer Sultan − *Department of Physics, University of Agriculture Faisalabad, Faisalabad 38040, Pakistan*

Muhammad Saleem − *Department of Physics, University of Agriculture Faisalabad, Faisalabad 38040, Pakistan*

Moustafa A. Rizk − *Empty Quarter Research Unit, Department of Chemistry, Faculty of Science and Arts at Sharurah, Najran University, Sharurah 68342, Saudi Arabia*

Muhammad Irfan − *Electrical Engineering Department, College of Engineering, Najran University Saudi Arabia, Najran 61441, Saudi Arabia*; orcid.org/0000-0003-4161-6875

Complete contact information is available at: https://pubs.acs.org/10.1021/acsomega.3c09207

Notes

The authors declare no competing financial interest.

■ ACKNOWLEDGMENTS

This research was funded by the Deanship of Scientific Research, Najran University, Kingdom of Saudi Arabia, under the National Research Priorities and Najran Area Research funding program grant code (NU/NRP/SERC/12/27).

■ REFERENCES

(1) Abou Elmaaty, T. M.; Elsisi, H.; Elsayad, G.; Elhadad, H.; Plutino, M. R. Recent advances in functionalization of cotton fabrics with Nanotechnology. *Polymers* **2022**, *14* (20), 4273.

(2) Asif, A. K. M. A. H.; Hasan, M. Z. Application of nanotechnology in modern textiles: A review. *Int. J. Curr. Eng. Technol.* **2018**, *8* (02), 227−231.

(3) Shah, M. A.; Pirzada, B. M.; Price, G.; Shibiru, A. L.; Qurashi, A. Applications of nanotechnology in smart textile industry: A critical review. *J. Adv. Res.* **2022**, *38*, 55−75.

(4) Al Bakri, H.; Abu Elhaija, W.; Al Zyoud, A. Solar photovoltaic panels performance improvement using active self-cleaning nanotechnology of SurfaShield G. *Energy* **2021**, *223*, 119908.

(5) Pakdel, E.; Wang, J.; Kashi, S.; Sun, L.; Wang, X. Advances in photocatalytic self-cleaning, superhydrophobic and electromagnetic interference shielding textile treatments. *Adv. Colloid Interface Sci.* **2020**, *277*, 102116.

(6) Ghobashy, M. M. Combined ultrasonic and gamma-irradiation to prepare TiO_2@ PET-g-PAAc fabric composite for self-cleaning application. *Ultrason. Sonochem.* **2017**, *37*, 529−535.

(7) Abbas, M.; Iftikhar, H.; Malik, M. H.; Nazir, A. Surface coatings of TiO_2 nanoparticles onto the designed fabrics for enhanced self-cleaning properties. *Coatings* **2018**, *8* (1), 35.

(8) Mahltig, B.; Zhang, J.; Wu, L.; Darko, D.; Wendt, M.; Lempa, E.; Rabe, M.; Haase, H. Effect pigments for textile coating: a review of the broad range of advantageous functionalization. *J. Coat. Technol. Res.* **2017**, *14*, 35−55.

(9) Bonet Aracil, M. Á.; Monllor, P.; Capablanca, L.; Gisbert, J.; Díaz, P.; Montava, I. A comparison between padding and bath exhaustion to apply microcapsules onto cotton. *Cellulose* **2015**, *22*, 2117−2127.

(10) Dihom, H. R.; Al-Shaibani, M. M.; Radin Mohamed, R. M. S.; Al-Gheethi, A. A.; Sharma, A.; Khamidun, M. H. B. Photocatalytic degradation of disperse azo dyes in textile wastewater using green zinc oxide nanoparticles synthesized in plant extract: A critical review. *J. Water Proc. Eng.* **2022**, *47*, 102705.

(11) Shahidi, S.; Rezaee, H.; Rashidi, A.; Ghoranneviss, M. In situ synthesis of ZnO Nanoparticles on plasma treated cotton fabric utilizing durable antibacterial activity. *J. Nat. Fibers* **2018**, *15* (5), 639−647.
(12) Wang, C.; Lv, J.; Ren, Y.; Zhou, Q.; Chen, J.; Zhi, T.; Lu, Z.; Gao, D.; Ma, Z.; Jin, L. Cotton fabric with plasma pretreatment and ZnO/Carboxymethyl chitosan composite finishing for durable UV resistance and antibacterial property. *Carbohydr. Polym.* **2016**, *138*, 106−113.
(13) Li, D.; Wang, R.; Liu, X.; Fang, S.; Sun, Y. Shear-thickening fluid using oxygen-plasma-modified multi-walled carbon nanotubes to improve the quasi-static stab resistance of Kevlar fabrics. *Polymers* **2018**, *10* (12), 1356.
(14) Shanmugam, L.; Kazemi, M. E.; Rao, Z.; Lu, D.; Wang, X.; Wang, B.; Yang, L.; Yang, J. Enhanced mode I fracture toughness of UHMWPE fabric/thermoplastic laminates with combined surface treatments of polydopamine and functionalized carbon nanotubes. *Composites, Part B* **2019**, *178*, 107450.
(15) Naz, M. Y.; Shukrullah, S.; Rehman, S. U.; Khan, Y.; Al-Arainy, A. A.; Meer, R. Optical characterization of non-thermal plasma jet energy carriers for effective catalytic processing of industrial wastewaters. *Sci. Rep.* **2021**, *11*, 2896.
(16) Saleem, M.; Naz, M. Y.; Shukrullah, S.; Ali, S.; Hamdani, S. T. A. Ultrasonic biosynthesis of TiO_2 nanoparticles for improved self-cleaning and wettability coating of DBD plasma pre-treated cotton fabric. *Appl. Phys. A: Mater. Sci. Process.* **2021**, *127*, 608.
(17) Irfan, M.; Hussain, H.; Saleem, B.; Saleem, M.; Shukrullah, S.; Legutko, S.; Petrů, J.; Naz, M. Y.; Pagáč, M.; Rahman, S.; Khan, R. Evaluation of Ultrasonically ZnO Loading Effect on Photocatalytic Self-Cleaning, UV Protection and Antibacterial Activity of Plasma/Citric Acid-Activated Cotton Fabric. *Nanomaterials* **2022**, *12* (12), 2122.
(18) Saleem, M.; Naz, M. Y.; Shukrullah, S.; Shujah, M. A.; Ullah, S.; Al-Sehemi, A. G. Statistical optimization of open air dielectric barrier discharge plasma effect on self-cleaning activity of ultrasonically Cu_2O/TiO_2-coated cotton fabric. *Appl. Phys. A: Mater. Sci. Process.* **2021**, *127*, 776.
(19) Irfan, M.; Naz, M. Y.; Saleem, M.; Tanawush, M.; Głowacz, A.; Glowacz, W.; Rahman, S.; Mahnashi, M. H.; Alqahtani, Y. S.; Alyami, B. A.; Alqarni, A. O.; Alsaiari, M. A. Statistical study of nonthermal plasma-assisted ZnO coating of cotton fabric through ultrasonic-assisted green synthesis for improved self-cleaning and antimicrobial properties. *Materials* **2021**, *14* (22), 6998.
(20) Çakır, B. A.; Budama, L.; Topel, Ö.; Hoda, N. Synthesis of ZnO nanoparticles using PS-b-PAA reverse micelle cores for UV protective, self-cleaning and antibacterial textile applications. *Colloids Surf., A* **2012**, *414*, 132−139.
(21) Ahmad, I.; Shukrullah, S.; Naz, M. Y.; Rasheed, M. A.; Ahmad, M.; Ahmed, E.; Akhtar, M. S.; Khalid, N. R.; Hussain, A.; Khalid, S. Boosted hydrogen evolution activity from Sr doped ZnO/CNTs nanocomposite as visible light driven photocatalyst. *Int. J. Hydrogen Energy* **2021**, *46* (53), 26711−26724.
(22) Seidelmann, L. J.; Bradley, J. W.; Ratova, M.; Hewitt, J.; Moffat, J.; Kelly, P. Reel-to-reel atmospheric pressure dielectric barrier discharge (DBD) plasma treatment of polypropylene films. *Appl. Sci.* **2017**, *7* (4), 337.
(23) Rodrigues, F.; Abdollahzadehsangroudi, M.; Nunes-Pereira, J.; Páscoa, J. Recent Developments on Dielectric Barrier Discharge (DBD) Plasma Actuators for Icing Mitigation. *Actuators* **2023**, *12* (1), 5.
(24) Pakdel, E.; Daoud, W. A. Self-cleaning cotton functionalized with TiO_2/SiO_2: focus on the role of silica. *J. Colloid Interface Sci.* **2013**, *401*, 1−7.
(25) Hebeish, A. A.; Abdelhady, M. M.; Youssef, A. M. TiO_2 nanowire and TiO_2 nanowire doped Ag-PVP nanocomposite for antimicrobial and self-cleaning cotton textile. *Carbohydr. Polym.* **2013**, *91* (2), 549−559.
(26) Thirumalai, K.; Shanthi, M.; Swaminathan, M. Hydrothermal fabrication of natural sun light active Dy_2WO_6 doped ZnO and its enhanced photo-electrocatalytic activity and self-cleaning properties. *RSC Adv.* **2017**, *7* (13), 7509−7518.
(27) Wu, Y.; Zhou, Z.; Tuo, Y.; Wang, K.; Huang, M.; Huang, Y.; Shen, S. A transparent $CNTs/TiO_2$ composite film with super-hydrophobic and photocatalytic functions self-assembled by liquid-phase deposition. *Mater. Chem. Phys.* **2015**, *149*−*150*, 522−529.
(28) Elçin, S.; Çılgı, G. K.; Bayrakdar, A.; Deligöz, H. The synthesis and characterization of azocalix[4]arene based chemosensors and investigation of their properties. *Spectrochim. Acta, Part A* **2015**, *142*, 178−187.
(29) Dakroury, G. A.; El-Shazly, E. A. A.; Hassan, H. S. Preparation and characterization of ZnO/Chitosan nanocomposite for Cs (I) and Sr (II) sorption from aqueous solutions. *J. Radioanal. Nucl. Chem.* **2021**, *330* (1), 159−174.
(30) Hoon Seo, K.; Markus, J.; Soshnikova, V.; Oh, K. H.; Anandapadmanaban, G.; Elizabeth Jimenez Perez, Z.; Mathiyalagan, R.; Kim, Y. J.; Yang, D. C. Facile and green synthesis of zinc oxide particles by Stevia Rebaudiana and its in vitro photocatalytic activity. *Inorg. Nano-Met. Chem.* **2019**, *49* (1), 1−6.
(31) Rojas, J. V.; Toro-Gonzalez, M.; Molina-Higgins, M. C.; Castano, C. E. Facile radiolytic synthesis of ruthenium nanoparticles on graphene oxide and carbon nanotubes. *Mater. Sci. Eng. B* **2016**, *205*, 28−35.
(32) Geetha, M.; Maurya, M. R.; Al-maadeed, S.; Muthalif, A. A.; Sadasivuni, K. K. High-precision nonenzymatic electrochemical glucose sensing based on CNTs/CuO nanocomposite. *J. Electron. Mater.* **2022**, *51* (9), 4905−4917.
(33) Selvaraj, S.; Palanivel, B.; Patrick, S.; Krishna Mohan, M.; Navaneethan, M.; Ponnusamy, S.; Muthamizhchelvan, C. Effect of Sr doping in ZnO microspheres for solar light-driven photodegradation of organic pollutants. *J. Mater. Sci.: Mater. Electron.* **2022**, *33*, 8777−8788.
(34) Park, B. H.; Park, H.; Kim, T.; Yoon, S. J.; Kim, Y.; Son, N.; Kang, M. S-scheme assisted Cu_2O/ZnO flower-shaped heterojunction catalyst for breakthrough hydrogen evolution by water splitting. *Int. J. Hydrogen Energy* **2021**, *46* (77), 38319−38335.
(35) Savari, R.; Rouhi, J.; Fakhar, O.; Kakooei, S.; Pourzadeh, D.; Jahanbakhsh, O.; Shojaei, S. Development of photo-anodes based on strontium doped zinc oxide-reduced graphene oxide nanocomposites for improving performance of dye-sensitized solar cells. *Ceram. Int.* **2021**, *47* (22), 31927−31939.
(36) Akram, R.; Almohaimeed, Z. M.; Bashir, A.; Ikram, M.; Qadir, K. W.; Zafar, Q. Synthesis and characterization of pristine and strontium-doped zinc oxide nanoparticles for methyl green photo-degradation application. *Nanotechnology* **2022**, *33* (29), 295702.
(37) Cursaru, L. M.; Valsan, S. N.; Puscasu, M. E.; Tudor, I. A.; Zarnescu-Ivan, N.; Vasile, B. S.; Piticescu, R. M. Study of ZnO-CNT Nanocomposites in High-Pressure Conditions. *Materials* **2021**, *14* (18), 5330.
(38) Saad, R.; Gamal, A.; Zayed, M.; Ahmed, A. M.; Shaban, M.; BinSabt, M.; Rabia, M.; Hamdy, H. Fabrication of ZnO/CNTs for application in CO_2 sensor at room temperature. *Nanomaterials* **2021**, *11* (11), 3087.
(39) Peña-Garcia, R.; Guerra, Y.; Castro-Lopes, S.; Camejo, Y. M.; Soares, J. M.; Franco, A.; Padrón-Hernández, E.; Cabrera-Baez, M. Morphological, magnetic and EPR studies of ZnO nanostructures doped and co-doped with Ni and Sr. *Ceram. Int.* **2021**, *47* (20), 28714−28722.
(40) Qi, K.; Xin, J. H.; Daoud, W. A.; Mak, C. L. Functionalizing polyester fiber with a self-cleaning property using anatase TiO_2 and low-temperature plasma treatment. *Int. J. Appl. Ceram. Technol.* **2007**, *4* (6), 554−563.
(41) Laohaprapanon, S.; Vanderlipe, A. D.; Doma, B. T., Jr.; You, S. J. Self-cleaning and antifouling properties of plasma-grafted poly (vinylidene fluoride) membrane coated with ZnO for water treatment. *J. Taiwan Inst. Chem. Eng.* **2017**, *70*, 15−22.
(42) Li, X.; Gao, Z.; Li, B.; Zhang, X.; Li, Y.; Sun, J. Self-healing superhydrophobic conductive coatings for self-cleaning and humidity-insensitive hydrogen sensors. *Chem. Eng. J.* **2021**, *410*, 128353.

https://doi.org/10.1021/acsomega.3c09207
ACS Omega 2024, 9, 1977−1989

(43) Ashraf, M.; Champagne, P.; Campagne, C.; Perwuelz, A.; Dumont, F.; Leriche, A. Study the multi self-cleaning characteristics of ZnO nanorods functionalized polyester fabric. *J. Ind. Text.* **2016**, *45* (6), 1440−1456.
(44) Venkatesan, S.; Suresh, S.; Ramu, P.; Arumugam, J.; Thambidurai, S.; Pugazhenthiran, N. Methylene blue dye degradation potential of zinc oxide nanoparticles bioreduced using Solanum trilobatum leaf extract. *Results Chem.* **2022**, *4*, 100637.
(45) Adeleke, J. T.; Theivasanthi, T.; Thiruppathi, M.; Swaminathan, M.; Akomolafe, T.; Alabi, A. B. Photocatalytic degradation of methylene blue by ZnO/$NiFe_2O_4$ nanoparticles. *Appl. Surf. Sci.* **2018**, *455*, 195−200.
(46) Elmorsi, T. M.; Elsayed, M. H.; Bakr, M. F. Enhancing the removal of methylene blue by modified ZnO nanoparticles: kinetics and equilibrium studies. *Can. J. Chem.* **2017**, *95* (5), 590−600.
(47) Trandafilović, L.; Jovanović, D.; Zhang, X.; Ptasińska, S.; Dramićanin, M. Enhanced photocatalytic degradation of methylene blue and methyl orange by ZnO: Eu nanoparticles. *Appl. Catal., B* **2017**, *203*, 740−752.
(48) Rehan, M.; Barhoum, A.; Khattab, T. A.; Gätjen, L.; Wilken, R. Colored, photocatalytic, antimicrobial and UV-protected viscose fibers decorated with Ag/Ag_2 CO_3 and Ag/Ag_3 PO_4 nanoparticles. *Cellulose* **2019**, *26*, 5437−5453.
(49) Khan, I.; Saeed, K.; Zekker, I.; Zhang, B.; Hendi, A. H.; Ahmad, A.; Ahmad, S.; Zada, N.; Ahmad, H.; Shah, L. A.; Shah, T.; Khan, I. Review on methylene blue: its properties, uses, toxicity and photodegradation. *Water* **2022**, *14* (2), 242.

https://doi.org/10.1021/acsomega.3c09207
ACS Omega 2024, 9, 1977−1989